Article

Synthesis of Quantum-Sized Cubic ZnS Nanorods by the Oriented Attachment Mechanism

Jung Ho Yu, Jin Joo, Hyun Min Park, Sung-Il Baik, Young Woon Kim, Sung Chul Kim, and Taeghwan Hyeon

J. Am. Chem. Soc., **2005**, 127 (15), 5662-5670• DOI: 10.1021/ja044593f • Publication Date (Web): 23 March 2005

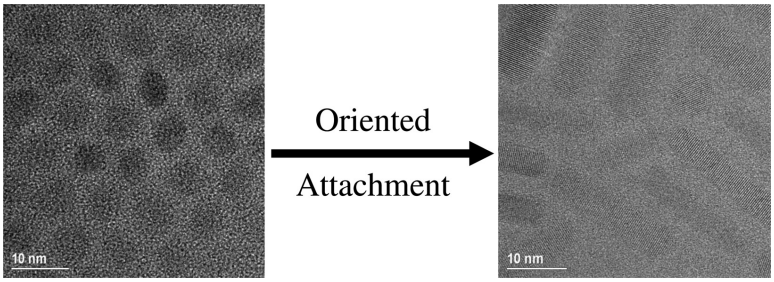

More About This Article

Additional resources and features associated with this article are available within the HTML version:

- Supporting Information
- Links to the 28 articles that cite this article, as of the time of this article download
- Access to high resolution figures
- Links to articles and content related to this article
- Copyright permission to reproduce figures and/or text from this article

View the Full Text HTML

J|A|C|S
ARTICLES
Published on Web 03/23/2005

Synthesis of Quantum-Sized Cubic ZnS Nanorods by the Oriented Attachment Mechanism

Jung Ho Yu,[†] Jin Joo,[†] Hyun Min Park,[‡] Sung-Il Baik,[§] Young Woon Kim,[§] Sung Chul Kim,[†] and Taeghwan Hyeon*,[†]

Contribution from the National Creative Research Initiative Center for Oxide Nanocrystalline Materials and School of Chemical and Biological Engineering, Seoul National University, Seoul 151-744, Korea, New Material Evaluation Center, Korea Research Institute of Standards and Science, Taejon 305-600, Korea, and School of Materials Science and Engineering, Seoul National University, Seoul 151-744, Korea

Received September 7, 2004; E-mail: thyeon@plaza.snu.ac.kr

Abstract: Quantum-sized ZnS nanocrystals with quasi-spherical and rod shapes were synthesized by the aging reaction mixtures containing diethylzinc, sulfur, and amine. Uniform-sized ZnS nanorods with the average dimension of 5 nm × 21 nm, along with a small fraction of 5 nm-sized quasi-spherical nanocrystals, were synthesized by adding diethylzinc to a solution containing sulfur and hexadecylamine at 125 °C, followed by aging at 300 °C. Subsequent secondary aging of the nanocrystals in oleylamine at 60 °C for 24 h produced nearly pure nanorods. Structural characterizations showed that these nanorods had a cubic zinc blende structure, whereas the fabrication of nanorods with this structure has been known to be difficult to achieve via colloidal chemical synthetic routes. High-resolution TEM images and reaction studies demonstrated that these nanorods are formed from the oriented attachment of quasi-spherical nanocrystals. Monodisperse 5 nm-sized quasi-spherical ZnS nanocrystals were separately synthesized by adding diethylzinc to sulfur dissolved in a mixture of hexadecylamine and 1-octadecene at 45 °C, followed by aging at 300 °C. When oleic acid was substituted for hexadecylamine and all other procedures were unchanged, we obtained 10 nm-sized quasi-spherical ZnS nanocrystals, but with broad particle size distribution. These two different-sized quasi-spherical ZnS nanocrystals showed different proportions of zinc blende and wurtzite crystal structures. The UV absorption spectra and photoluminescence excitation spectra of the 5 nm ZnS quasi-spherical nanocrystals and of the nanorods showed a blue-shift from the bulk band-gap, thus showing a quantum confinement effect. The photoluminescence spectra of the ZnS nanorods and quasi-spherical nanocrystals showed a well-defined excitonic emission feature and size- and shape-dependent quantum confinement effects.

Introduction

Nanocrystalline materials have attracted tremendous attention from researchers in many disciplines.[1,2] These nanocrystals exhibit novel electronic, magnetic, optical, chemical, and mechanical properties, which make them highly attractive for many important technological applications. Of the various types of nanocrystals, semiconducting metal chalcogenide nanocrystals have been the most intensively studied because of their quantum confinement effects and size- and shape-dependent photoemission characteristics.[3] These semiconductor nanocrystals have been applied to many different technological areas, including biological labeling and diagnostics, light emitting diodes, photovoltaic devices, and lasers.[4] Many semiconducting nanocrystals of metal sulfides with various compositions and shapes have been synthesized.[5] ZnS is a wide band-gap semiconductor with a band-gap energy (E_g) of 3.6 eV. For many years, ZnS materials doped with various metal ions have been used as

[†] School of Chemical and Biological Engineering, Seoul National University.
[‡] Korea Research Institute of Standards and Science.
[§] School of Materials Science and Engineering, Seoul National University.

(1) (a) Schmid, G. *Nanoparticles: From Theory to Application*; Wiley-VCH: Weinheim, Germany, 2004. (b) Klabunde, K. J. *Nanoscale Materials in Chemistry*; Wiley-Interscience: New York, 2001. (c) Fendler, J. H. *Nanoparticles and Nanostructured Films*; Wiley-VCH: Weinheim, Germany, 1998. (d) Zhang, J. Z.; Wang, Z.-L.; Liu, J.; Chen, S.; Liu, G.-Y. *Self-Assembled Nanostructures*; Kluwer Academic/Plenum Publishers: New York, 2003. (e) Rogach, A. L.; Talapin, D. V.; Shevchenko, E. V.; Kornowski, A.; Haase, M.; Weller, H. *Adv. Funct. Mater.* **2002**, *12*, 653.
(2) (a) Sun, S.; Murray, C. B.; Weller, D.; Folks, L.; Moser, A. *Science* **2000**, *287*, 1989. (b) Hyeon, T. *Chem. Commun.* **2003**, 927. (c) Nirmal, M.; Brus, L. E. *Acc. Chem. Res.* **1999**, *32*, 407. (d) Klimov, V. I.; Mihkailovsky, A.; Xu, S.; Malko, A.; Hollingsworth, J.; Leatherdale, C.; Bawendi, M. G. *Science* **2000**, *290*, 314. (e) Dumestre, F.; Chaudret, B.; Amiens, C.; Renaud, P.; Fejes, P. *Science* **2004**, *303*, 821.
(3) (a) Murray, C. B.; Norris, D. J.; Bawendi, M. G. *J. Am. Chem. Soc.* **1993**, *115*, 8706. (b) Peng, X.; Wickham, J.; Alivisatos, A. P. *J. Am. Chem. Soc.* **1998**, *120*, 5343. (c) Peng, X.; Manna, L.; Yang, W.; Wickham, J.; Scher, E.; Kadavanich, A.; Alivisatos, A. P. *Nature* **2000**, *404*, 59. (d) Manna, L.; Scher, E. C.; Alivisatos, A. P. *J. Am. Chem. Soc.* **2000**, *122*, 12700. (e) Peng, Z. A.; Peng, X. *J. Am. Chem. Soc.* **2001**, *123*, 183. (f) Peng, Z. A.; Peng, X. *J. Am. Chem. Soc.* **2001**, *123*, 1389. (g) Peng, Z. A.; Peng, X. *J. Am. Chem. Soc.* **2002**, *124*, 3343. (h) Manna, L.; Milliron, D. J.; Scher, E. C.; Alivisatos, A. P. *Nat. Mater.* **2003**, *2*, 382. (i) Milliron, D. J.; Hughes, S. M.; Cui, Y.; Manna, L.; Li, J.; Wang, L.-W.; Alivisatos, A. P. *Nature* **2004**, *430*, 190. (j) Peng, X. *Chem.—Eur. J.* **2002**, *8*, 335. (k) Alivisatos, A. P. *Science* **1996**, *271*, 933. (l) Murray, C. B.; Kagan, C. R.; Bawendi, M. G. *Science* **1995**, *270*, 1335. (m) Kim, S.; Fisher, B. R.; Eisler, H.-J.; Bawendi, M. G. *J. Am. Chem. Soc.* **2003**, *125*, 11466. (n) Talapin, D. V.; Rogach, A. L.; Kornowski, A.; Haase, M.; Weller, H. *Nano Lett.* **2001**, *1*, 207. (o) Eychmüller, A. *J. Phys. Chem. B* **2000**, *104*, 6514.

10.1021/ja044593f CCC: $30.25

phosphors for displays. Recently, nanostructured doped ZnS materials have attracted considerable attention because of their superior luminescence characteristics as compared to those of their bulk counterparts.[6] Several different synthetic routes have been investigated for the production of ZnS nanostructures.[7,8] However, high-quality ZnS nanocrystals having uniform particle size, shape, and good optical properties have rarely been reported. In most of the previous studies, ZnS nanocrystals having broad size distribution and poor optical quality have been synthesized.

One-dimensional (1-D) nanocrystalline materials, including nanorods and nanowires, have been intensively studied because of their unique properties, which are derived from their low dimensionality.[9] There have been several reports on the synthesis of ZnS nanorods and nanowires using high-temperature thermal evaporation procedures and template-synthetic routes.[8] Most of these 1-D ZnS nanocrystals have diameters larger than that required for the emergence of quantum confinement effect. In comparison, many 1-D semiconductor nanocrystals in the quantum confinement regime have been synthesized through the surfactant-controlled rod-growth approach.[3c−j,10] However, the 1-D synthesis of semiconductor nanocrystals by this approach is mainly limited to hexagonal structured materials. In materials having hexagonal crystal structure, the difference in the surface energy between the (0001) lattice plane and the other planes is large enough to induce anisotropic growth along the [0001] direction, whereas this is not the case for materials having cubic crystal structure because of its highly symmetric crystal structure.[10a] Usually, ZnS has a cubic zinc blende structure below 1020 °C, but at higher temperature, the hexagonal wurtzite crystal structure predominates. This is why the 1-D ZnS nanocrystal is difficult to achieve via colloidal synthetic routes. The solid−liquid−solution (SLS) growth method has been successfully applied to cubic-structured InAs nanorods and InP nanowires,[10] but the shape-controlled synthesis of ZnS has not been previously reported. Herein, we report the synthesis of uniform and quantum-sized quasi-spherical ZnS nanocrystals and nanorods from the oriented attachment process. Both the quasi-spherical nanocrystals and nanorods exhibit well-defined excitonic emission, and the optical properties of these nanocrystals are discussed.

Experimental Section

1-Hexadecylamine (HDA, 98%), diethylzinc (1 M solution in hexane), elemental sulfur powder, 1-octadecene (ODE, tech. grade), oleylamine (70%, tech. grade), oleic acid (90%, tech. grade), and 2-(4-biphenylyl)-5-phenyl-1,3,4-oxadiazole (PBD) were purchased from Aldrich Chemical Co. HPLC grade solvents, including dichloromethane, hexane, cyclohexane, and ethanol were purchased from J. T. Baker. Trioctylphosphine oxide (TOPO, 90%, Strem) was distilled under vacuum before use. Synthesis was conducted under an argon atmosphere using standard Schlenk techniques.

Synthesis of ZnS Nanorods. Five grams of 1-hexadecylamine (HDA, 21 mmol) was degassed under vacuum at 100 °C for 1 h. Then, 3 mmol (0.096 g) of elemental sulfur dissolved in HDA was heated to 125 °C in an argon atmosphere. Diethylzinc (0.5 mmol) was then rapidly injected into the sulfur solution at 125 °C. The resulting solution was heated to 300 °C and held at this temperature for 1 h. The reaction mixture was then cooled to 60 °C, and 50 mL of ethanol was added to precipitate the ZnS nanocrystals. The resulting precipitate was retrieved by centrifugation and washed several times with ethanol to remove excess HDA, yielding yellow colored ZnS nanocrystals composed mostly of nanorods with a small portion of quasi-spherical nanocrystals. To increase the yield of the nanorods, the ZnS nanocrystals were placed in 5 g of degassed oleylamine and aged at 60 °C for 1 day.

Synthesis of Quasi-Spherical ZnS Nanocrystals. The following procedure was used to synthesize 5 nm-sized quasi-spherical ZnS nanocrystals. HDA (2.5 g, 10 mmol) and 2.5 g of 1-octadecene (ODE, 10 mmol) were mixed and degassed under vacuum at 100 °C for 1 h. Then, 3 mmol (0.096 g) of elemental sulfur was dissolved in the HDA/ODE mixture in an argon atmosphere, and the temperature was decreased to 45 °C. Diethylzinc (0.5 mmol) was then injected into the sulfur solution at 45 °C. The resulting reaction mixture was slowly heated to 300 °C and held at this temperature for 2 h. As the temperature increased, the solution color changed from green to yellow and finally to red. The reaction mixture was then cooled to 60 °C, and 50 mL of 1-butanol was added to precipitate the ZnS nanocrystals. The precipitate was retrieved by centrifugation and washed several times with ethanol to remove excess HDA and ODE. Next, 10 nm quasi-spherical ZnS nanocrystals were synthesized using a similar procedure, except that 2.5 g of ODE (10 mmol) and 2.76 g of oleic acid (9.76 mmol) were used instead of HDA.

Characterization of the Nanocrystals. The nanocrystals were characterized by low- and high-resolution TEM and X-ray diffraction. Low-resolution TEM images were obtained on a JEOL EM-2010 microscope. High-resolution TEM (HRTEM) images were obtained using a JEOL JEM-3000F microscope. The TEM image simulation was done using a java version of an electron microscopy image simulation (JEMS) program using a multi-slice simulation calculation. Synchrotron X-ray diffraction data were collected on the 8C2 beam

(4) (a) Coe, S.; Woo, W.-K.; Bawendi, M. G.; Bulovic, V. *Nature* **2002**, *420*, 800. (b) Achermann, M.; Petruska, M. A.; Kos, S.; Smith, D. L.; Koleske, D. D.; Klimov, V. I. *Nature* **2004**, *429*, 642. (c) Huynh, W. U.; Dittmer, J. J.; Alivisatos, A. P. *Science* **2002**, *295*, 2425. (d) Alivisatos, A. P. *Nat. Biotechnol.* **2004**, *22*, 47. (e) Kim, S.; Lim, Y. T.; Soltesz, E. G.; De Grand, A. M.; Lee, J.; Nakayama, A.; Parker, J. A.; Mihaljevic, T.; Laurence, R. G.; Dor, D. M.; Cohn, L. H.; Bawendi, M. G.; Frangioni, J. V. *Nat. Biotechnol.* **2004**, *22*, 93.

(5) (a) Jun, Y.; Lee, S.-M.; Kang, N.-J.; Cheon, J. *J. Am. Chem. Soc.* **2001**, *123*, 5150. (b) Jun, Y.; Jung, Y.; Cheon, J. *J. Am. Chem. Soc.* **2002**, *124*, 615. (c) Lee, S.-M.; Jun, Y.; Cheon, J. *J. Am. Chem. Soc.* **2002**, *124*, 11244. (d) Larsen, T. H.; Sigman, M. B., Jr.; Ghezelbash, A.; Doty, R. C.; Korgel, B. A. *J. Am. Chem. Soc.* **2003**, *125*, 5638. (e) Ghezelbash, A.; Sigman, M. B., Jr.; Korgel, B. A. *Nano Lett.* **2004**, *4*, 537. (f) Pradhan, N.; Katz, B.; Efrima, S. *J. Phys. Chem. B* **2003**, *107*, 13843.

(6) (a) Bhargava, R. N.; Gallagher, D.; Hong, X.; Nurmikko, A. *Phys. Rev. Lett.* **1994**, *72*, 416. (b) Sooklal, K.; Cullum, B. S.; Angel, S. M.; Murphy, C. J. *J. Phys. Chem.* **1996**, *100*, 4551. (c) Suyver, J. F.; Wuister, S. F.; Kelly, J. J.; Meijerink, A. *Nano Lett.* **2001**, *1*, 429. (d) Dinsmore, A. D.; Hsu, D. S.; Gray, H. F.; Qadri, S. B.; Tian, Y.; Ratna, B. R. *Appl. Phys. Lett.* **1999**, *75*, 802.

(7) (a) Zhong, X.; Liu, S.; Zhang, Z.; Li, L.; Wei, Z.; Knoll, W. *J. Mater. Chem.* **2004**, *14*, 2790. (b) Nanda, J.; Sapra, S.; Sarma, D. D.; Chandrasekharan, N.; Hodes, G. *Chem. Mater.* **2000**, *12*, 1018. (c) Khitrov, G. A.; Strouse, G. F. *J. Am. Chem. Soc.* **2003**, *125*, 10465. (d) Wageh, S.; Shu-Man, L.; You, F. T.; Xu-Rong, X. *J. Lumin.* **2003**, *102*−*103*, 768. (e) Wageh, S.; Ling, Z. S.; Xu-Rong, X. *J. Cryst. Growth* **2003**, *255*, 332. (f) Zhao, Y.; Zhang, Y.; Zhu, H.; Hadjipanayis, G. C.; Xiao, J. Q. *J. Am. Chem. Soc.* **2004**, *126*, 6874.

(8) (a) Ma, C.; Moore, D.; Li, J.; Wang, Z. L. *Adv. Mater.* **2003**, *15*, 228. (b) Chen, X.; Xu, H.; Xu, N.; Zhao, F.; Lin, W.; Lin, G.; Fu, Y.; Huang, Z.; Wang, H.; Wu, M. *Inorg. Chem.* **2003**, *42*, 3100. (c) Barrelet, C. J.; Wu, Y.; Bell, D. C.; Lieber, C. M. *J. Am. Chem. Soc.* **2003**, *125*, 11498. (d) Jiang, X.; Xie, Y.; Lu, J.; Zhu, L.; He, W.; Qian, Y. *Chem. Mater.* **2001**, *13*, 1213. (e) Zhu, Y.-C.; Bando, Y.; Xue, D.-F.; Goldberg, D. *J. Am. Chem. Soc.* **2003**, *125*, 16196. (f) Zhu, Y.-C.; Bando, Y.; Xue, D.-F.; Goldberg, D. *Adv. Mater.* **2004**, *16*, 831. (g) Li, Y.; Li, X.; Yang, C.; Li, Y. *J. Phys. Chem. B* **2004**, *108*, 16002.

(9) (a) Xia, Y.; Yang, P.; Sun, Y.; Wu, Y.; Mayers, B.; Gates, B.; Yin, Y.; Kim, F.; Yan, H. *Adv. Mater.* **2003**, *15*, 353. (b) Hu, J.; Li, L.-S.; Yang, W.; Manna, L.; Wang, L. W.; Alivisatos, A. P. *Science* **2001**, *292*, 2060. (c) Wang, J.; Gudiksen, M. S.; Duan, X.; Cui, Y.; Lieber, C. M. *Science* **2001**, *293*, 1455. (d) Hu, J.-T.; Odom, T. W.; Lieber, C. M. *Acc. Chem. Res.* **1999**, *32*, 435. (e) Lee, S.-M.; Cho, S.-N.; Cheon, J. *Adv. Mater.* **2003**, *15*, 441. (f) Holmes, D.; Doty, R. C.; Johnston, K. P.; Korgel, B. A. *Science* **2000**, *287*, 1471. (g) Hanrath, T.; Korgel, B. A. *J. Am. Chem. Soc.* **2002**, *124*, 1424. (h) Park, J.; Koo, B.; Hwang, Y.; Bae, C.; An, K.; Park, J.-G.; Park, H. M.; Hyeon, T. *Angew. Chem., Int. Ed.* **2004**, *43*, 2282.

(10) (a) Kan, S.; Mokari, T.; Rothenberg, E.; Banin, U. *Nat. Mater.* **2003**, *2*, 155. (b) Yu, H.; Li, J.; Loomis, R. A.; Wang, L.-W.; Buhro, W. E. *Nat. Mater.* **2003**, *2*, 517. (c) Kan, S.; Aharoni, A.; Mokari, T.; Banin, U. *Faraday Discuss.* **2004**, *125*, 23.

line at the Pohang Light Source (Korea). A Si(111) crystal was used as a monochromator for the incident beam, and the wavelength of 0.15425 nm was calibrated using a Si standard. The data were collected over the 2θ range of $10° \sim 135°$ using a 0.025° step size. Rietveld refinement for the synchrotron X-ray data was performed using the Fullprof 2K program.[11] A pseudo-Voigt function was used as the peak profile for the refinement. Elemental analysis of the ZnS nanocrystals was performed by X-ray photoelectron spectroscopy (XPS) using a Sigma Probe (ThermoVG, U.K.) electron spectroscope for chemical analysis (ESCA) and an Al anode as a monochromatic X-ray source. The optical properties of the ZnS nanocrystals were characterized by electronic absorption and fluorescence spectroscopy. Electronic absorption and fluorescence spectra were obtained using a Perkin-Elmer Lambda Model 20 UV−vis spectrometer and a JASCO FP750 spectrofluorometer, respectively. Quantum yields were measured using 2-(4-biphenylyl)-5-phenyl-1,3,4-oxadiazole (PBD), which has an absorption maximum at 303 nm and a quantum yield of 83% when excited with a 313 nm UV laser, as a standard.[12]

Results and Discussion

Synthesis of Rod-Shaped ZnS Nanocrystals. The current synthetic procedure is a modified version of the method used by our group for the synthesis of monodisperse nanocrystals of metals, oxides, and sulfides, which involves the mixing of precursors and surfactants at low temperature followed by aging at high temperature.[13] In our previous report on the generalized synthesis of uniform-sized sulfide nanocrystals, we used metal chloride and elemental sulfur as reagents.[14] In contrast, in the present synthesis, we employed diethylzinc instead of zinc chloride as a zinc precursor. As will be discussed later, employing diethylzinc allowed the formation of nanocrystals with relatively few deep-trap sites, which resulted in enhanced band-edge emission properties.

Rod-shaped ZnS nanocrystals (nanorods) were synthesized by adding diethylzinc to a solution of sulfur in hexadecylamine (HDA) at 125 °C, followed by aging at 300 °C. TEM showed that the product was composed of 80% rods and 20% spheres (Figure 1a). To increase the proportion of the ZnS nanorods, the product was further aged in oleylamine at 60 °C for 24 h. The overall synthetic process is described in Scheme 1. The TEM image after the secondary aging in oleylamine showed that most of the nanocrystals were rod-shaped, and that the average size of the nanorods was 5 nm (diameter) × 21 nm (length), with a diameter standard deviation of 18% and a length standard deviation of 35% (Figure 1b−d). Electron-diffraction (ED) patterns and high-magnification TEM images showed that the nanorods had a cubic zinc blende structure (Figure 2). Furthermore, the HRTEM images revealed that the interplanar distance along the growth axis was 0.311 nm, which is consistent with the interplanar distance of the (111) plane of the cubic zinc blende structure of ZnS, thus confirming that the nanorods' elongation axis was in the [111] direction. In the current synthesis, nearly pure ZnS nanorods were formed from the kinetic control of the reaction condition in the first step of the synthesis, followed by the oriented attachment of the ZnS

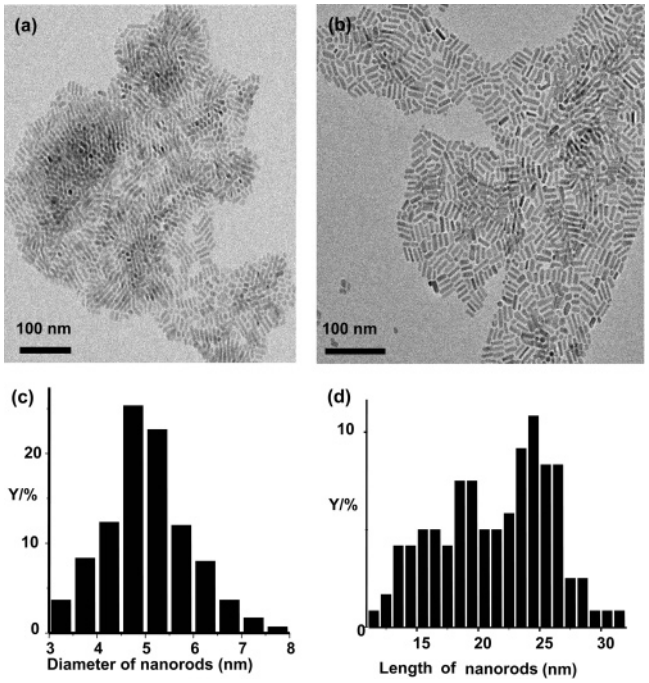

Figure 1. (a) TEM image of as-synthesized ZnS nanorods containing some fraction of spherical nanocrystals. (b) TEM image of ZnS nanorods obtained after the secondary aging at 60 °C. (c and d) Size distribution histograms of ZnS nanorods obtained from counting 500 nanorods. (c) Diameter distribution histogram of ZnS nanorods. (d) Length distribution histogram of ZnS nanorods.

Scheme 1. Overall Synthetic Procedure for the Nanorods[a]

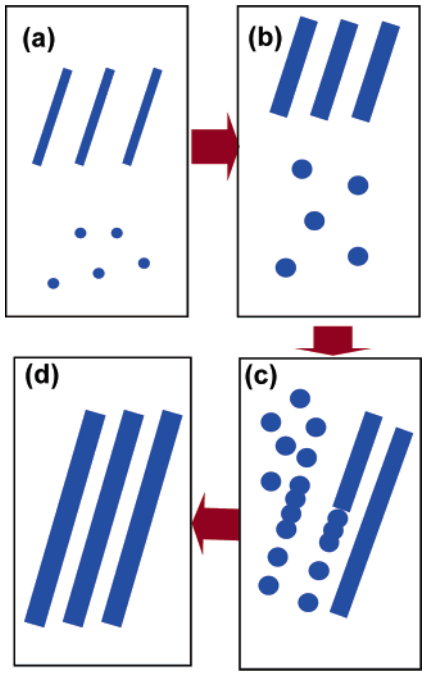

[a] (a and b) The first step of nanorod synthesis. (a) Kinetic formation of short nanorods, (b) intraparticle ripening. (c and d) The secondary aging at 60 °C in oleylamine. (c) Oriented attachment of the 5 nm-sized quasi-spherical nanocrystals to form elongated nanorods. (d) Ostwald ripening to form smooth surface nanorods.

(11) Rodriguez-Carvajal, *FULLPROF 2K*, Program for the Rietveld Refinement, Laboratory Leon Brillouin (CEA-CNRS), 2000.
(12) Berlman, I. B. *Handbook of Fluorescence Spectra of Molecules*; Academic Press: New York, 1971.
(13) (a) Hyeon, T.; Lee, S. S.; Park, J.; Chung, Y.; Na, H. B. *J. Am. Chem. Soc.* **2001**, *123*, 12798. (b) Joo, J.; Yu, T.; Kim, Y. W.; Park, H. M.; Wu, F.; Zhang, J. Z.; Hyeon, T. *J. Am. Chem. Soc.* **2003**, *125*, 6553. (c) Kim, S. W.; Park, J.; Jang, Y.; Chung, Y.; Hwang, S.; Hyeon, T.; Kim, Y. W. *Nano Lett.* **2003**, *3*, 1289. (d) Son, S. U.; Jang, Y.; Park, J.; Na, H. B.; Park, H. M.; Yun, H. J.; Lee, J.; Hyeon, T. *J. Am. Chem. Soc.* **2004**, *126*, 5026. (e) Son, S.; Park, I. K.; Park, J.; Hyeon, T. *Chem. Commun.* **2004**, 778. (f) Park, J.; An, K.; Hwang, Y.; Park, J.-G.; Noh, H.-J.; Kim, J.-Y.; Park, J.-H.; Hwang, N.-M.; Hyeon, T. *Nat. Mater.* **2004**, *3*, 891.
(14) Joo, J.; Na, H. B.; Yu, T.; Yu, J. H.; Kim, Y. W.; Wu, F.; Zhang, J.; Hyeon, T. *J. Am. Chem. Soc.* **2003**, *125*, 11100.

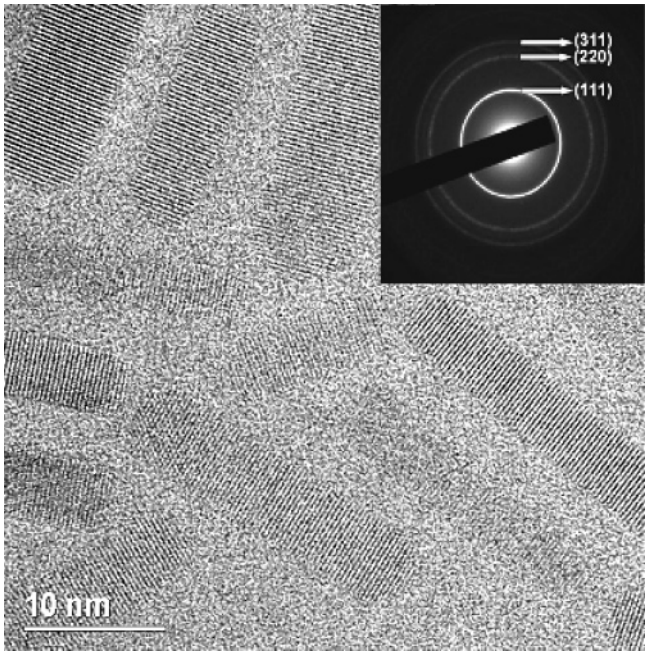

Figure 2. High-resolution TEM image of ZnS nanorods. Inset is electron diffraction pattern of ZnS nanorods.

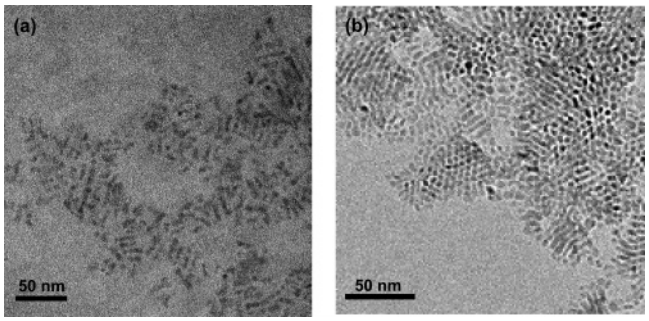

Figure 3. (a) ZnS nanorods which are formed at 220 °C. (b) ZnS nanorods after the first synthetic step (after aging at 300 °C for 1 h).

nanocrystals in the second aging in oleylamine at 60 °C. During this attachment process, the ZnS nanocrystals coalesce to form secondary rod-shaped particles, in which the (111) planes of the ZnS nanocrystals are almost perfectly aligned, as was shown by the TEM images.[15] In Figure 1d, the length distribution histogram showed a maximum peak at every 5 nm. This phenomenon is due to the oriented attachment of quasi-spherical nanocrystals with a mean diameter of 5 nm, and a similar phenomenon was reported by Weller and co-workers for ZnO nanorods.[15h]

In the first step of our nanorod synthesis, nanorods seem to be formed by the high chemical potential resulted from the high monomer concentration. As shown in the Figure 3a, thin nanorods with diameters of 3 nm mixed with 3 nm-sized spherical nanocrystals were produced at the sample taken at 220 °C. However, the reaction system seems to fail at maintaining high chemical potential (i.e., high monomer concentration) because 1-hexadecylamine (HDA) surfactant is not a strong ligand. As a result, initially formed 3 nm-sized nanorods seemed to undergo an intraparticle ripening process, producing thicker 5 nm-sized nanorods, as shown in the TEM image in Figure 3b. In addition, 5 nm-sized quasi-spherical nanocrystals seemed to be produced from the ripening of the initial 3 nm-sized quasi-spherical nanocrystals after the first step of the nanorod synthesis (Figure 3b).[3f]

During the second step of the synthesis, involving aging in oleylamine, the remaining quasi-spherical nanoparticles, which were generated in the first step, are attached to one another and to preformed nanorods to produce nanorods at a temperature as low as 60 °C. In the final stage of the nanorod growth via the oriented attachment process, Ostwald ripening smoothens the irregular surface of nanorods to produce nanorods with smooth surface. As a result, more nanorods with large diameters were generated, exhibiting an asymmetric diameter histogram (Figure 1c). These results are very interesting because ZnS nanorods with cubic zinc blende structure were formed from the oriented attachment growth of spherical cubic ZnS nanocrystals.[15f] As far as we know, this is the first report on the synthesis of 1-D nanorods with a cubic crystal structure that was achieved via the oriented attachment mechanism.

We optimized various synthetic conditions in order to synthesize ZnS nanorods. We used thermally labile diethylzinc as the precursor and optimized the injection temperature. At an injection temperature >150 °C, large numbers of polydisperse spherical nanocrystals were synthesized. On the other hand, at an injection temperature <150 °C, ZnS nanorods were predominantly produced. The optimum injection temperature for the nanorod synthesis was found to be between 100 and 130 °C, where nanorods with good crystallinity were obtained in high yield. The choice of an appropriate surfactant was also essential for the success of the procedure. When strongly binding surfactants, such as trioctylphosphine oxide (TOPO), were employed in the synthesis, no nanorods were produced, but rather polydisperse and shapeless nanocrystals larger than 5 nm were generated (Supporting Information). This was probably because TOPO binds too strongly to the zinc sites and inhibits 1-D growth. Hexadecylamine, which has an intermediate binding strength, was identified as the best surfactant for the synthesis of ZnS nanorods.[16] In addition, large excess of sulfur, with a zinc to sulfur molar ratio of 1:6, was used in the synthesis. When a smaller amount of sulfur was used, smaller spherical nanocrystals were produced rather than nanorods. In the previous report on the mechanism study of CdSe nanorod formation reported by Peng and co-workers,[3g] the initial cadmium-to-selenium ratio was essential to maintain high chemical potential. When the cadmium precursor was used in excess, pure CdSe nanorods were formed. In contrast, when the selenium precursor was used in excess, spherical CdSe nanocrystals were generated. Interestingly, in our previous report on the synthesis of CdS nanocrystals, the reaction of excess sulfur generated CdS nanorods.[14] These results imply that the less reactive species should be employed in excess to maintain high chemical potential and, consequently, to produce rod-shaped chalcogenide nanocrystals. In the current case, because elemental sulfur is less reactive than diethylzinc, sulfur was added in excess to

(15) (a) Penn, R. L.; Banfield, J. F. *Science* **1998**, *281*, 969. (b) Penn, R. L.; Banfield, J. F. *Am. Mineral.* **1999**, *84*, 871. (c) Penn, R. L.; Banfield, J. F. *Geochim. Cosmochim. Acta* **1999**, *63*, 1549. (d) Zhang, H.; Banfield, J. F. *Am. Mineral.* **1999**, *84*, 528. (e) Park, S.-J.; Kim, S.; Lee, S.; Khim, Z. G.; Char, K.; Hyeon, T. *J. Am. Chem. Soc.* **2000**, *122*, 8581. (f) Huang, F.; Zhang, H.; Banfield, J. F. *Nano Lett.* **2003**, *3*, 373. (g) Huang, F.; Zhang, H.; Banfield, J. F. *J. Phys. Chem. B* **2003**, *107*, 10470. (h) Pacholski, C.; Kornowski, A.; Weller, H. *Angew. Chem., Int. Ed.* **2002**, *41*, 1188.

(16) (a) Hines, M. A.; Guyot-Sionnest, P. *J. Phys. Chem. B* **1998**, *102*, 3655. (b) Norris, D. J.; Yao, N.; Charnock, F. T.; Kennedy, T. A. *Nano Lett.* **2001**, *1*, 3.

maintain high chemical potential and, consequently, to form the nanorods. Furthermore, the use of a large amount of sulfur turned out to be important for the synthesis of ZnS nanocrystals with good optical properties, as will be discussed later.

During the secondary aging in oleylamine at 60 °C, the remaining spherical nanocrystals were transformed to nanorods via oriented attachment. The substitution of strongly hindered HDA with more compact oleylamine, which is known to act as a C-8 hydrocarbon chain via cis-conformation,[17] seems to induce the facile coalescence of the spherical nanocrystals to form nanorods. The growth of nanorods via this secondary aging at low temperature is similar to the synthesis of CdTe nanowires via the oriented attachment of spherical CdTe nanoparticles resulting from the partial removal of surfactant by aging at room temperature, as reported by Kotov and co-workers.[18] Similar to their report, the secondary growth of nanorods is caused by the dipole−dipole attraction of preformed ZnS nanocrystals. They suggested that one-dimensional nanostructure could be formed by the oriented attachment mechanism when the energy of dipole attraction among nanocrystals is higher than or comparable to the thermal energy, *kT*. To prove this, the aging temperature in oleylamine is varied from 60 to 300 °C. When the preformed ZnS nanocrystals by the first step of nanorod synthesis were aged in oleylamine at 300 °C (Supporting Information), ZnS nanorods with shorter length and the same diameter of 5 nm were produced compared to those aged at 60 °C. This seems to result from the predominance of thermal energy of the high temperature of 300 °C over dipole−dipole attraction and further demonstrates that low temperature aging in an appropriate surfactant induces facile coalescence of nanocrystals to form one-dimensional structure.

Previous reports by the Banfield group showed that the oriented attachment of ZnS nanocrystals occurs without directional preference under hydrothermal conditions.[15f] The major difference between our result and those previously reported involves the introduction of an amine surfactant. Amine seems to selectively adsorb to the (110) facet of ZnS nanocrystals and minimize its energy, thus enhancing the surface energy difference between (110) and (111) facets. We speculate that this enhancement of surface energy differences by facet selective amine ligand adsorption is the underlying reason for the oriented attachment of ZnS nanocrystals in one direction.

Synthesis of Quasi-Spherical ZnS Nanocrystals. Quasi-spherical ZnS nanocrystals were synthesized by adding diethylzinc to sulfur dissolved in the mixture of hexadecylamine (HDA) and 1-octadecene (ODE) at 45 °C, followed by aging of the reaction mixture at 300 °C. Whereas only HDA was used in the synthesis of the ZnS nanorods, in this case, HDA was diluted with ODE,[19] and the injection temperature was decreased, which allowed the controlled nucleation and growth of the nanocrystals. This injection of precursor into diluted coordinating solvent at moderately low temperature and subsequent aging at higher temperature is consistent with the syntheses of monodisperse nanocrystals previously reported by our group.[13]

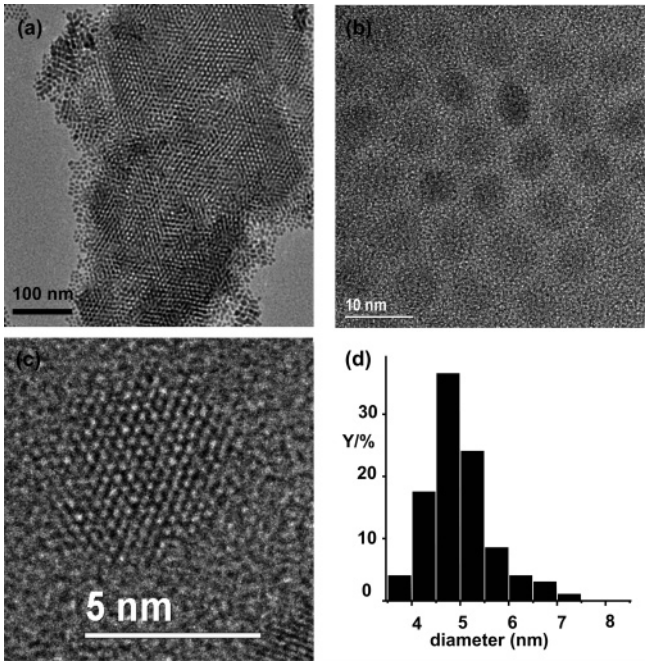

Figure 4. (a) Low-magnification TEM image of self-assembled 5 nm quasi-spherical ZnS nanocrystals. (b) High-magnification TEM image of self-assembled 5 nm quasi-spherical ZnS nanocrystals. (c) High-resolution transmission electron microscope (HRTEM) image of a 5 nm quasi-spherical nanocrystal. (d) Diameter distribution histogram of 5 nm quasi-spherical ZnS nanocrystals obtained from counting 300 nanocrystals.

The TEM images of the nanocrystals, shown in Figure 4a,b, revealed an extensive 2-D and 3-D close-packed structure, demonstrating a highly uniform particle size distribution (standard deviation of <10% and <5% when agglomerated particles are excluded, Figure 4d). The HRTEM images of the 5 nm-sized nanocrystals (Figure 4c) revealed their highly crystalline nature and mostly zinc blende structure. When oleylamine was substituted for hexadecylamine and all other procedures were kept unchanged, the same 5 nm-sized quasi-spherical ZnS nanocrystals were obtained. However, the isolated quasi-spherical nanocrystals underwent oriented attachment when they were redispersed in organic solvents, such as hexane (Figure 5). For example, when 5 nm quasi-spherical ZnS nanocrystals stabilized with oleylamine were kept in hexane at room temperature for 1 day, nanorods with dimensions of 5 nm × 10−15 nm were generated (Figure 5b). When the solution was further aged for 30 days, nanorods with 5 nm thick nanocrystals were formed (Figure 5c). These results provide additional proof of the oriented attachment driven by oleylamine. In contrast, the 5 nm quasi-spherical ZnS nanocrystals stabilized with hexadecylamine remained stable and were to be kept stable indefinitely in hexane at room temperature. However, when it was aged in excess oleylamine at 60 °C, as in the second step of nanorod synthesis, 5 nm diameter ZnS nanorods were produced predominantly, which further confirms the formation of the nanorods via the oriented attachment of spherical ZnS nanocrystals (Figure 6).

When oleic acid was substituted for hexadecylamine and all the other synthetic procedures were kept unchanged, we obtained 10 nm-sized quasi-spherical ZnS nanocrystals. Figure 7 shows a TEM image of these 10 nm-sized quasi-spherical nanocrystals with 25% size distribution, which is broader than that of the 5.0 nm nanocrystals. These results can be understood based on

(17) Dumestre, F.; Chaudret, B.; Amiens, C.; Fromen, M. C.; Casanove, J.; Renaud, P.; Zurcher, P. *Angew. Chem., Int. Ed.* **2002**, *41*, 4286.
(18) Tang, Z.; Kotov, N. A.; Giersig, M. *Science* **2002**, *297*, 237.
(19) (a) Yu, W. W.; Peng, X. *Angew. Chem., Int. Ed.* **2002**, *41*, 2368. (b) Battaglia, D.; Peng, X. *Nano Lett.* **2002**, *2*, 1027. (c) Li, L. S.; Pradhan, N.; Wang, Y.; Peng, X. *Nano Lett.* **2004**, *4*, 2261. (d) Jana, N. R.; Chen, Y.; Peng, X. *Chem. Mater.* **2004**, *16*, 3931.

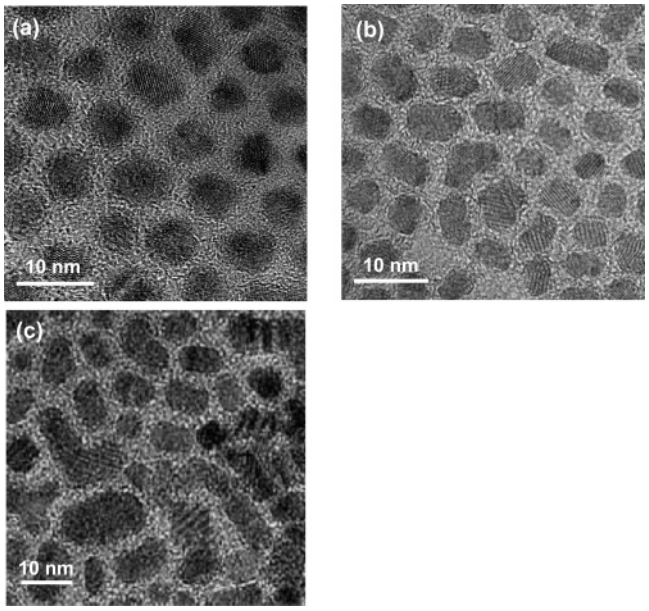

Figure 5. TEM image of 5 nm quasi-spherical ZnS nanocrystals synthesized using oleylamine: (a) as-synthesized sample, (b) after keeping hexane solution at room temperature for 1 day, (c) after keeping in a hexane solution at room temperature for 30 days.

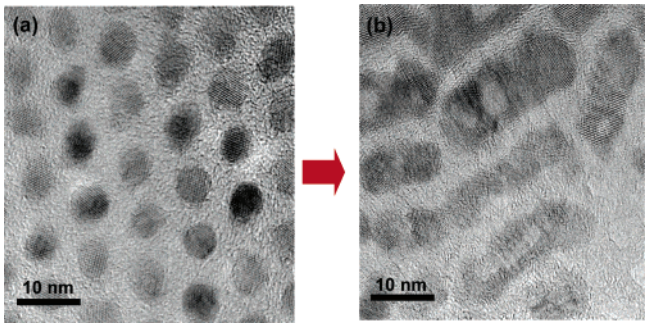

Figure 6. (a) Image of 5 nm ZnS nanocrystals coordinated by HDA. (b) Nanorods produced from the aging of 5 nm-sized ZnS nanocrystals in oleylamine at 60 °C.

the different binding abilities of the two surfactants. By only one cycle of size selection process, we obtained 10 nm-sized quasi-spherical ZnS nanocrystals with very narrow size distribution (Supporting Information). We synthesized the 10 nm-sized quasi-spherical ZnS nanocrystals in order to compare their optical properties with those of the quantum-sized 5 nm ZnS nanocrystals and nanorods, even though the nanocrystals were of poor quality in terms of their particle size distribution.

Crystal Structures of ZnS Nanocrystals. Figure 8 shows powder X-ray diffraction (XRD) patterns of the ZnS nanocrystals. The XRD patterns revealed that the quasi-spherical nanocrystals were composed of a mixture comprising a majority zinc blende and a small amount of wurtzite. Moreover, the quasi-spherical nanocrystals with different sizes showed different proportions of these two crystal structures. It was difficult to differentiate the zinc blende crystal phase from the wurtzite by using the X-ray diffraction pattern only. Consequently, Rietveld refinement was carried out to determine the crystal structures. All of the X-ray data could be successfully refined with cubic zinc blende and hexagonal wurtzite crystal structure models. The weight fractions of each phase in the samples were derived from the refinement results. The relation between the weight

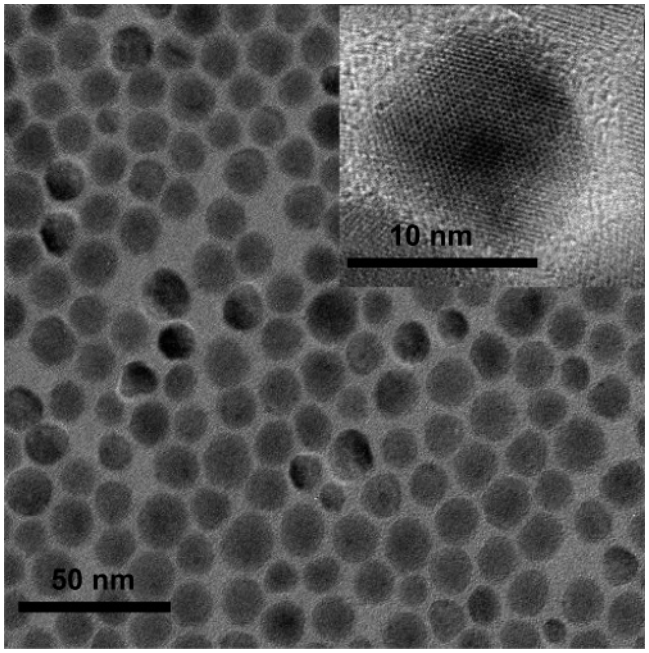

Figure 7. TEM image of 10 nm quasi-spherical ZnS nanocrystals. The inset is the HRTEM image of 10 nm quasi-spherical nanocrystals.

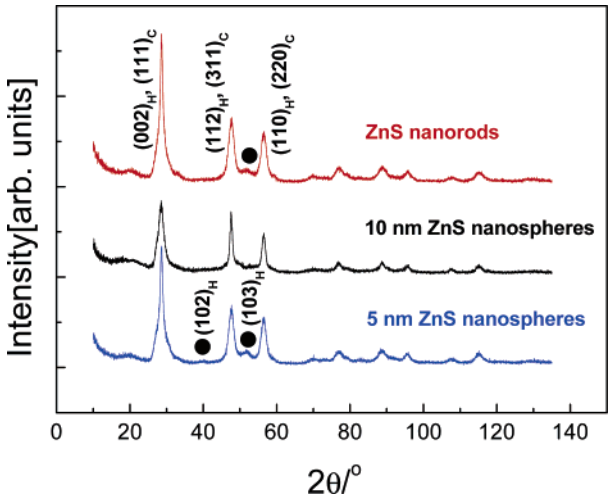

Figure 8. X-ray diffraction patterns of ZnS nanocrystals: 5 nm quasi-spherical ZnS nanocrystals (blue curve), 10 nm quasi-spherical ZnS nanocrystals (black curve), and ZnS nanorods (red curve). The black dots indicate wurtzite peaks.

fraction of one phase and the other parameters are as follows:

$$W_p = \frac{S_p(ZMV)_p}{\sum_i S_i(ZMV)_i} \quad (1)$$

where, S, Z, M, and V are the Rietveld scale factor, the number of formula units per unit cell, the mass of the formula unit, and the unit cell volume, respectively.[20]

The refinement results showed that the 5 nm-sized ZnS nanocrystals comprised 79% zinc blende crystal structure and 21% wurtzite crystal structure, whereas 10 nm-sized quasi-spherical nanocrystals comprised 98% zinc blende crystal structure and only 2% wurtzite crystal structure. Although the

(20) Hill, R. J.; Howard, C. J. *J. Appl. Crystallogr.* **1987**, *20*, 467.

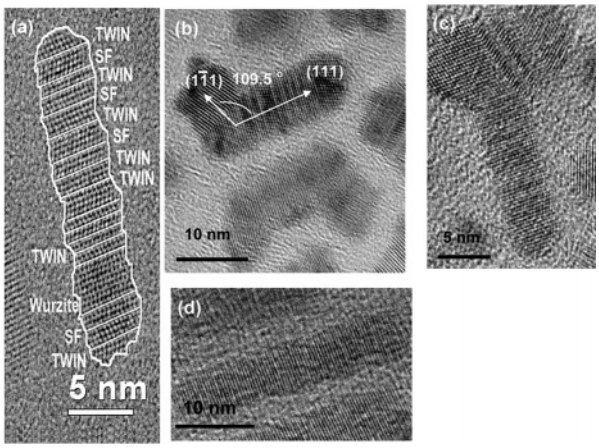

Figure 9. HRTEM images of (a) a ZnS nanorod, (b) bipod-shaped and Π-shaped ZnS nanocrystals, (c) a tripod-shaped ZnS nanocrystal, and (d) a peapod-like-structured ZnS nanorod. "Twin" means twinning defects; "SF" means stacking faults, and "Wurtzite" means wurtzite faults.

phase transition temperature from zinc blende to wurtzite of bulk ZnS is 1020 °C, recent reports have shown that this phase transition temperature may be lowered as nanocrystal size decreases.[7f,21,22] A theoretical prediction and subsequent experimental verification showed that zinc blende structure has surface energy higher than that of the wurtzite structure in the nanoscale regime.[22c,d] Consistent with this prediction, our results show that the ratio of the two crystal phases depends on nanocrystal size. However, the ZnS nanorods produced by the secondary aging process were made up of 82.1% zinc blende crystal structure and 17.9% wurtzite crystal structure. From the crystallographic viewpoint, we speculate that the oriented attachment is fundamentally driven by the higher surface energy of the 5 nm zinc blende nanocrystals. In other words, the high surface energy of the 5 nm quasi-spherical nanocrystals with predominantly zinc blende structure was relieved by the reduction in the surface-to-volume ratio afforded by the formation of the nanorods, and consequently the driving force for the phase transformation to wurtzite structure seemed to be significantly diminished in our synthesis condition.

Figure 9 shows HRTEM images of the ZnS nanorods. In these images, we observed several common features of oriented attachment growth. These include stacking faults, twinning defects, and wurtzite faults, which were formed by the (111) plane oriented coalescence of the initial ZnS nanocrystals leading to various branched nanostructures, such as bipods, tripods, and Π-shaped nanocrystals (Figure 9b,c). These planar defects were further confirmed by the crystal structure simulation of the HRTEM image (Supporting Information). Also, undulated peapod-like structures, which are intermediate nanorod species, were observed to be formed by the oriented attachment of several quasi-spherical nanocrystals (Figure 9d).

Optical Properties of ZnS Nanocrystals. Figure 10a shows the UV absorption spectra of the 5 nm-sized quasi-spherical ZnS nanocrystals and the nanorods. Both the quasi-spherical

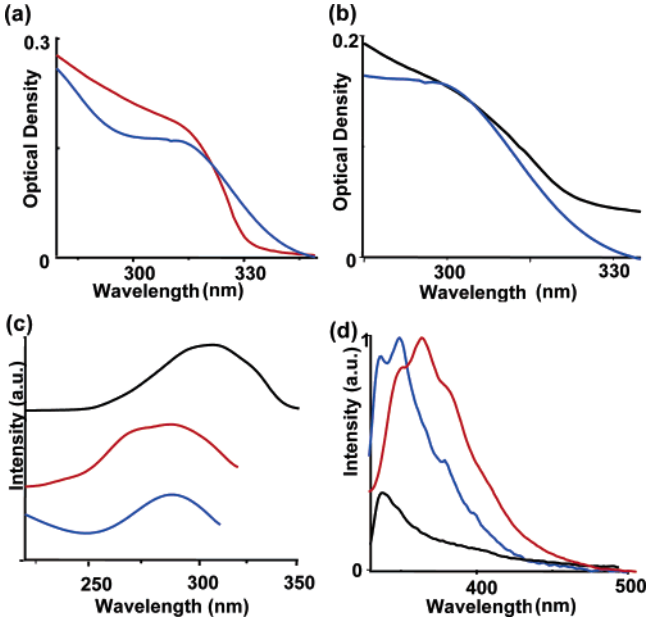

Figure 10. (a) Comparison of UV spectra of 5 nm quasi-spherical nanocrystals (blue line) with nanorods (red line). (b) Comparison of UV spectra of 5 nm quasi-spherical nanocrystals with 10 nm quasi-spherical nanocrystals (black line). (c) Photoluminescence excitation (PLE) spectra of ZnS nanocrystals. (d) Photoluminescence (PL) spectra of ZnS nanocrystals.

nanocrystals and the nanorods show an absorption band at 310 nm, which was blue-shifted from the bulk band-gap wavelength of 340 nm. The long absorption tail in the case of the 5 nm spherical ZnS nanocrystals was due to scattering by the crystals. According to the report by Wageh and co-workers on studies of the change of absorption spectra of ZnS nanocrystals by increasing the reflux time of the ZnS nanocrystal growth solution,[7e] the absorption band at 310 nm in our samples seems to result from the defect sites and the peak from the excitonic transition seems to be hidden in the absorption band at 310 nm. In their study, they observed that the absorption band at 320 nm decreased and the intensity of the absorption peak at 295 nm increased as the refluxing time increased. Consequently, they concluded that the crystallinity of ZnS nanocrystals increased by increasing the refluxing time, the band at 320 nm was caused by a large concentration of defect sites (vacancies and interstitial ions), and the absorption maximum at 295 nm is an excitonic (band-to-band) transition in ZnS nanocrystals. Furthermore, the absorption spectrum of 10 nm quasi-spherical ZnS nanocrystals in Figure 10b also shows a blue-shifted absorption band from the bulk band-gap of ZnS, but there is no significant absorption band difference between 5 nm ZnS nanocrystals and 10 nm ZnS nanocrystals, although 10 nm-sized ZnS nanocrystals are in a weak confinement size regime.

To find the position for the excitonic transition of our ZnS nanocrystals, photoluminescence excitation (PLE) spectra were obtained (Figure 10c). Using the wavelength of the maximum PL intensity, the PLE spectrum was recorded in the 220−350 nm (PLE) range. The recorded PLE spectra show that the maximum excitation occurs at around 290 nm for both 5 nm quasi-spherical nanocrystals and 5 nm diameter ZnS nanorods. This maximum excitation wavelength is in good agreement with the Wageh et al. previous result of the UV absorption maximum peak at 295 nm.

(21) Chen, C.-C.; Herhold, A. B.; Johnson, C. S.; Alivisatos, A. P. *Science* **1997**, *276*, 398.
(22) (a) Qadri, S. B.; Skelton, E. F.; Hsu, D.; Dinsmore, A. D.; Yang, J.; Gray, H. F.; Ratna, B. R. *Phys. Rev. B* **1999**, *60*, 9091. (b) Zhang, H.; Gilbert, B.; Huang, F.; Banfield, J. F. *Nature* **2003**, *424*, 1025. (c) Zhang, H.; Huang, F.; Gilbert, B.; Banfield, J. F. *J. Phys. Chem. B* **2003**, *107*, 13051. (d) Gilbert, B.; Huang, F.; Zhang, H.; Waychunas, G. A.; Banfield, J. F. *Science* **2004**, *30*, 651.

The Bohr diameter of bulk ZnS is about 5 nm, which is comparable to the diameter of the quasi-spherical nanocrystals and the nanorods, where moderate quantum confinement occurs. Considering that the diameters of the 5 nm quasi-spherical nanocrystals and the nanorods are nearly the same, the peak at around 290 nm wavelength in the PLE spectrum of the nanorods indicates that the quantum confinement of the nanorods mainly depends on the radial direction of the rods rather than the longitudinal direction.[3h,9b,23]

Although many studies have been conducted on the optical properties of ZnS nanocrystals, there have been few reports on the excitonic emission feature of ZnS nanocrystals.[7d,e,19c] In most cases, trap-state emission at around 450 nm is a dominant emission feature, regardless of the particle sizes or shapes. Furthermore, size- and shape-dependent emission characteristics caused by the quantum confinement effect have not been reported for ZnS nanocrystals. As shown in Figure 10d, the photoluminescence (PL) spectra of the ZnS nanorods and the 5 nm-sized quasi-spherical nanocrystals showed peak maxima at $<$400 nm, revealing a well-defined excitonic emission feature. The spectra were measured at the same excitation wavelength of 290 nm. While fluorescence intensity changed somewhat with excitation wavelength, the fluorescence peak position remained the same. These luminescence spectra show size- and shape-dependent quantum confinement effects. Photoluminescence spectra of the 5 nm-sized quasi-spherical nanocrystals showed inhomogeneous broadened peaks at 335 and 350 nm and weak shoulders at 380 and 400 nm, respectively. These peaks can be assigned to a band-edge emission (335 nm), shallow-donor and acceptor emission peaks (350 and 380 nm), and a deep-trap emission peak (400 nm). This emission behavior is consistent with a recent report on highly luminescent ZnS nanocrystals.[7e] To demonstrate the quantum confinement effect of the 5 nm-sized nanocrystals, a photoluminescence spectrum of the quasi-spherical 10 nm-sized nanocrystals was obtained. The PL spectrum of the quasi-spherical 10 nm-sized ZnS nanocrystals showed band-edge emission at 345 nm, which is homogeneously broadened at longer wavelength due to defect-related surface state (Figure 7b). Compared to the emission spectra of the 10 nm-sized ZnS nanocrystals, the band-edge emission spectra of the quasi-spherical 5 nm-sized nanocrystals were blue-shifted by approximately 110 meV. The emission spectrum of the ZnS nanorods showed a band-edge emission feature at 345 nm, shallow-donor and acceptor emission peaks at 360 and 380 nm, and a weak deep-trap emission feature at 420 nm. The band-edge emission of the ZnS nanorods (345 nm) was Stokes-shifted by 107 meV compared to that of the 5 nm quasi-spherical nanocrystals (335 nm).[9b] However, the two shallow-trap state emissions showed different behaviors depending on the energy gap between the shallow-trap and the band-edge. The shallow-trap emission of the ZnS nanorods (360 nm), which is close to the band-edge emission, showed almost the same Stokes shift of 98 meV as that of the 5 nm quasi-spherical nanocrystals (350 nm). In addition, the shallow-trap emission, which is far from the band-edge emission (380 nm), showed no Stokes shift at all. This implies that the shallow-trapped exciton also experienced shape-dependent quantum confinements as well as the exciton in the band-edge, depending on the degree of the energy gap between the band-edge and the shallow-trap.[24] The important characteristic of the emission spectra of the spherical nanocrystals and the nanorods is the absence of a deep-trap emission at around 450 nm, which is known to arise from surface sulfur vacant sites.

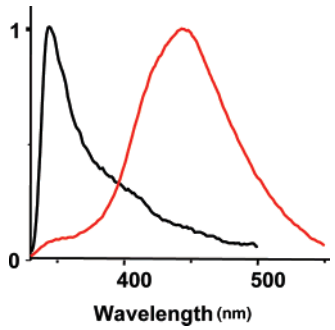

Figure 11. Comparison of photoluminescence spectra of the 10 nm quasi-spherical nanocrystals synthesized in the current report (black line), and 11 nm quasi-spherical ZnS nanocrystals made by our group using zinc chloride and stoichiometric sulfur as reagents (red line).

Figure 11 compares the normalized photoluminescence spectra of the 10 nm quasi-spherical nanocrystals and the 11 nm-sized spherical nanocrystals synthesized by our group using zinc chloride as a precursor.[14] As shown in this figure, the use of a large excess of sulfur in the current synthesis made it possible to synthesize ZnS nanocrystals with few sulfur vacant sites.[6c,25] Furthermore, the use of diethylzinc instead of zinc chloride seemed to induce the formation of ZnS nanocrystals without chlorine-derived defect sites.[26] Despite the large excess of sulfur used in the synthesis, the molar ratios of zinc to sulfur in the quasi-spherical nanocrystals and the nanorods as determined by X-ray photoelectron spectroscopy (XPS) were both 1.0:1.1, demonstrating that stoichiometric zinc sulfide (ZnS) was produced. Quantum yields were measured using 2-(4-biphenylyl)-5-phenyl-1,3,4-oxadiazole (PBD) as a standard, and the measured quantum yields of the quasi-spherical 5 nm-sized nanocrystals and the nanorods were 1.4 and 1.1%, respectively. These low quantum yields, despite the absence of deep-trap-state emission, might be due to a nonradiative pathway via a shallow-trap.

Conclusion

Quantum-sized ZnS nanocrystals with quasi-spherical and rod shapes were synthesized. The synthetic procedures offer several important characteristics for ZnS nanocrystals. First, ZnS nanorods with predominantly cubic zinc blende structure were obtained by the oriented attachment mechanism. Second, the shapes of the nanocrystals can easily be altered by changing the experimental parameters. Third, the synthesized nanocrystals exhibited the quantum confinement effect and a well-defined excitonic emission feature.

Acknowledgment. This work was supported by the National Creative Research Initiative Program of the Korean Ministry

(23) (a) Li, L.-S.; Hu, J.; Yang, W.; Alivisatos, A. P. *Nano Lett.* **2001**, *1*, 349. (b) Yu, H.; Li, J.; Loomis, R. A.; Gibbons, P. C.; Wang, L. W.; Buhro, W. E. *J. Am. Chem. Soc.* **2003**, *125*, 16168.

(24) (a) Pankove, J. I. *Optical Processes in Semiconductors*; Prentice Hall: Englewood Cliffs, NJ, 1971. (b) Spanhel, L.; Haase, M.; Weller, H.; Henglein, A. *J. Am. Chem. Soc.* **1987**, *109*, 5649. (c) Eychmüller, A.; Hässelbarth, A.; Katsikas, L.; Weller, H. *Ber. Bunsen-Ges. Phys. Chem.* **1991**, *95*, 79.

(25) Qu, L.; Peng, X. *J. Am. Chem. Soc.* **2002**, *124*, 2049.

(26) Ozawa, L.; Minoru, I. *Chem. Rev.* **2003**, *103*, 3835.

of Science and Technology. We would like to thank Dr. Fanxin Wu and Prof. Jin Z. Zhang at the University of California at Santa Cruz, and Mr. Hyunsuk Kim and Prof. Sangsig Kim at the Korea University for their very helpful discussion on the optical characterization. We also would like to thank Dr. Nam Soo Shin at Pohang Acceleration Laboratory for synchrotron powder X-ray diffraction measurements.

Supporting Information Available: TEM image of ZnS nanocrystals synthesized by adding 0.15 g of TOPO in the reaction mixture; TEM image of ZnS nanorods produced from the secondary aging in oleylamine at 300 °C; TEM image of 10 nm quasi-spherical nanocrystals obtained after one cycle of size selection process; crystal structure refinement data for the ZnS nanocrystals refined by Rietveld method; observed, calculated, and difference profiles for the ZnS nanorods and 5 nm quasi-spherical ZnS nanocrystals using a Rietveld refinement; HRTEM image and the corresponding simulated image of a single ZnS nanorod. This material is available free of charge via the Internet at http://pubs.acs.org.

JA044593F